Lightweight LIF-only SNN accelerator using differential time encoding

Daniel Windhager*, Lothar Ratschbacher†, Bernhard A. Moser**‡, Michael Lunglmayr§

arXiv:2505.11252v1 [cs.NE] 16 May 2025

***Abstract*—Spiking Neural Networks (SNNs) offer a promising solution to the problem of increasing computational and energy requirements for modern Machine Learning (ML) applications. Due to their unique data representation choice of using spikes and spike trains, they mostly rely on additions and thresholding operations to achieve results approaching state-of-the-art (SOTA) Artificial Neural Networks (ANNs). This advantage is hindered by the fact that their temporal characteristic does not map well to already existing accelerator hardware like GPUs. Therefore, this work will introduce a hardware accelerator architecture capable of computing feedforward LIF-only SNNs, as well as an accompanying encoding method to efficiently encode already existing data into spike trains. Together, this leads to a design capable of $> 99\%$ accuracy on the MNIST dataset, with $\approx 0.29ms$ inference times on a Xilinx Ultrascale+ FPGA, as well as $\approx 0.17ms$ on a custom ASIC using the open-source predictive 7nm ASAP7 PDK. Furthermore, this work will showcase the advantages of the previously presented differential time encoding for spikes, as well as provide proof that merging spikes from different synapses given in differential time encoding can be done efficiently in hardware.**

***Index Terms*—Spiking Neural Network, LIF-only, differential time, ASAP7, FPGA**

I. Introduction

THE field of Artificial Intelligence (AI) and more specifically ML is ever changing and growing, with a clear trend towards bigger and more expansive network architectures, which in turn means larger parameter spaces and datasets. While GPUs, faster memory and higher bandwidths can curb some of these issues, the fact remains that the most recent architectures, like the transformer-based GPT-4 [1], currently require large server infrastructure, for inference as well as for training. Because of the large computational effort involved, less computationally expensive architectures have gained interest in academia and industry in recent years. One of these approaches is to utilize SNNs instead of traditional ANNs, due to their improved power efficiency [2], sparsity characteristics [3] and, depending on the choice of the neuron model and spike encoding, decreased computational effort. This is especially important for embedded devices and edge applications, as these often impose hard limits on energy efficiency and inference time. Although they offer a promising solution, SNNs introduce a different set of problems, such as the need for choosing an appropriate encoding method for the data. Even more important, GPUs and CPUs are not well suited to the task of accelerating SNNs due to their asynchronous and event-based architecture, making efficient custom accelerator architectures essential. An additional issue is the encoding of vectorized data into spike sequences, which is less than obvious for SNNs. This issue of choosing the encoding can be mitigated by incorporating the encoding into the training process, thus allowing the network to adjust based on the training data. Furthermore, the custom hardware architecture presented here, which improves upon a previous design [4], allows for efficient processing of SNNs, especially on resource constrained Field-programmable Gate Arrays (FPGAs).

This work will extend both of these previously published concepts [5], by providing a mathematical proof of the main spike merger network structure, as well as providing justification for the differential time encoding chosen in this and previous works. Additionally, this work will highlight the universality of the concept of learned encoding, by showcasing its performance for the MNIST [6] and CIFAR10 [7] dataset. Finally, this work also provides synthesis results for the presented accelerator architecture for the Xilinx Ultrascale+ ZCU102 MPSoC board as well as for the open-source predictive 7nm ASAP7 PDK [8]. These results demonstrate that the proposed architecture can be implemented efficiently on resource constrained digital hardware while still being competitive in terms of accuracy and inference speed.

II. Background and related work

Many different works regarding SNNs have been proposed in the past, dealing with the theoretical and practical machine learning aspects as well as different architectures and designs capable of inference or even training the network using custom hardware. Although quite a few publications explore training and inference on GPUs [9]–[13], many only train on GPUs to then deploy the trained model on custom hardware such as FPGAs or even ASICs. A very prominent example is Intel's Loihi and Loihi 2 [14] architecture, with the second generation being capable of simulating more than 1 million neuron cores on the chip, with fully programmable neuron models and flexible routing between the neurons using a Network-on-Chip (NoC). Loihi is, contrary to many other architectures, even capable of on-chip learning, making it possible to use the same chip for training as well as inference. Other ASICs capable of SNN inference include the SpiNNaker 2 [15], [16]

*Intelligent Wireless Systems, Silicon Austria Labs, Linz, Austria, daniel.windhager@silicon-austria.com
†Intelligent Wireless Systems, Silicon Austria Labs, Linz, Austria, lothar.ratschbacher@silicon-austria.com
‡Institute of Signal Processing, Johannes Kepler University, JKU SAL IWS Lab, Linz, Austria, bernhard.moser@jku.at
**double affiliation: Software Competence Center Hagenberg (SCCH), 4232 Hagenberg, Austria
§Institute of Signal Processing, Johannes Kepler University, Linz, Austria, michael.lunglmayr@jku.at

which utilizes 152 parallel ARM cores with custom dedicated accelerators, connected by a flexible NoC to enable fast processing of sparse and non-sparse networks. While Loihi[1] and SpiNNaker are designed to handle various different networks and neuron models, there are also designs which optimize with a special use-case in mind, such as SparrowSNN [17]. It is designed specifically for detecting heart disease using the MIT-BIH dataset [18] and a custom 22nm ASIC for acceleration. Although there exist many ASIC designs specifically for acceleration of SNNs, even more designs use FPGAs for this task, due to their lower cost for small quantities and their reprogrammability. While many of them focus on energy-efficiency as the main selling criteria of SNNs [19]–[22], very few architectures focus on "pure" SNNs, i.e. networks which only include Leaky-Integrate and Fire (LIF) neurons. In fact, many publications combine regular ANNs, such as Convolutional Neural Networks (CNNs) or transformer based architectures with an activation layer consisting of LIF neurons [23]–[28], which somewhat diminishes the power efficiency aspect, since multipliers are once again necessary. To completely remove the necessity for multiplications, the neuron model must be chosen such that it can be computed with addition and shift operations only, which is why the authors of this work chose to realize their SNN networks using only an implementation-efficient variant of the LIF model. Additionally, many works that have been published in recent years use the Address Event Representation (AER) to represent spikes [29]–[32], resulting in a large overhead (specifically due to the choice of using absolute time to represent spikes), impairing power and computational efficiency. Here, as described below, we argue for using a more efficient differential time encoding.

III. Efficient spike representation

Many of the works using the AER, use absolute time to represent the time at which a spike or event occurred. However, this is not only suboptimal but can also lead to problems, especially for systems running continuously, as after some finite time the counter used to represent the current time will overflow. As an alternative, the authors proposed the differential time representation in [33] that can be shown to be almost equivalent, in terms of required bit length, to the absolute time representation in the worst case, whereas for most other cases it substantially reduces the bit width required to represent the same information. This is accomplished by encoding the time difference between a spike and its predecessor, instead of using the absolute time information. To represent spikes that occur at a time not representable with the specified bit width of the differential time, an overflow symbol is introduced (the highest representable number $2^b - 1$, where b is the chosen bit width), which signifies the passage of time without a spike.

To illustrate why the AER is not ideal, consider a spike train with $K \in \mathbb{N}$ spikes for which the last spike occurs at some time $T \in \mathbb{N}_0$. Using absolute time, $\lceil \log_2(T+1) \rceil$ bits are needed to represent every individual spike, whereas the differential time encoding depends on the distribution of the times between the spikes (that are typically smaller than the maximum time). Assuming for the moment that we do not wish to use more than one symbol to represent a single spike, i.e. we do not allow overflow symbols, then the worst case, where all K spikes occur at the latest possible moment, would also require a bit width of $\lceil \log_2(T+1) \rceil$. The best case for the differential time encoding method occurs when all K spikes are exactly evenly spaced, reducing the required bit width to $\lceil \log_2(\frac{T+1}{K}) \rceil$, thus giving a substantial improvement. The exact savings in terms of bit width depend heavily on the distribution of the spikes, however, even in the worst case the differential time representation at most devolves into the same performance as the absolute time representation. Notice that in the current discussion no overflow symbols have been considered. As will be shown next, the overflow symbols actually improve the efficiency of the differential time representation in terms of the required bit width.

A. Sampled time compared to differential time

Another possible way to represent spike trains is to simply sample the spike trains and use the resulting sequences of ones and zeros (assuming only positive spikes of amplitude one are used), which could be represented as

$$S = (s_1, s_2, ..., s_{n-1}), s_i \in \{0, 1\}. \tag{1}$$

This sampled version of the spike train is actually equivalent to the differential time representation, using only a single bit, with 1 as the spike amplitude, whereas 0 can be interpreted as overflow symbol signifying that one sampling time has passed where no spike was triggered. In the sampled version, a 0 signifies that at this point in time no spike occurred whereas a 1 signifies that a spike occured. In contrast, when using the differential time representation with a single bit, the value 0 indicates that a spike occurs in zero time, i.e. now, whereas the value 1 is the highest representable value and is thus used as the overflow symbol, signifying that no spike occurs at this moment in time.

Clearly, if spikes occur less often, a larger bit width for the differential time representation would yield an advantage over the sampled time representation, but it is not immediately obvious which bit width is ideal. Intuitively, a bit width that is too low for a given spike train produces a large number of overflow symbols thus reducing efficiency, whereas an exceedingly large bit width would never produce overflow symbols but wastes many bits on encoding a smaller time difference, as described previously. The most efficient bit width is dependent on the distribution of spikes in the spike trains one wants to encode. To be more precise, the overall distribution of the time differences between the spikes, determines the ideal bit width to choose. In order to properly optimize for this, we need a cost function to compare costs of different approaches. One candidate for this is to simply use $N_S b$, where N_S is the number of symbols required to

[1]Note that, at the time of writing Loihi is only available for research purposes by directly contacting the Intel Neuromorphic Research Community (NRC).

represent the entire spike train and b is the bit width of a single symbol. Using this cost function, it is simple to arrive at the optimal cost of encoding the spike train, by realizing that every difference $d_i \in \mathbb{N}_0$ for which $0 \leq d_i < 2^b - 1$ holds, can be represented with a single symbol. Similarly, every difference d_i for which $2^b - 1 \leq d_i < 2^{b+1} - 1$ holds, can be represented with two symbols, and so forth. In general, the number of symbols for a given time difference and bit width is $\lceil d_i/(2^b - 1) \rceil$. Therefore the total number of symbols for the entire spike train is

$$N_S(b) = \sum_i \left\lceil \frac{d_i}{2^b - 1} \right\rceil \tag{2}$$

leading to the overall bits required to encode the entire spike train as

$$B_S(b) = bN_S(b) = b \sum_i \left\lceil \frac{d_i}{2^b - 1} \right\rceil . \tag{3}$$

Ideally we would now like to find

$$b^* = \arg\min_{b \in \mathbb{N}} B_S(b) \tag{4}$$

which, due to the ceiling function, is unfortunately not possible to find analytically. It is however possible, and quite straightforward, to find a minimum by computing all values of $B_S(b)$ for practically relevant b-values. To do this, we first generate a histogram of all the differential time spikes that we wish to encode. An example of all the differential time spikes that occur in a 400-128-10 network using the MNIST test dataset can be seen in Fig. 1. Instead of having to iterate through all of the differences as given in (3), we now simply calculate the number of symbols required to encode each of the differential times in the histogram for a given bitwidth, which yields

$$B_S(b) = b \sum_i K_i \left\lceil \frac{i}{2^b - 1} \right\rceil \tag{5}$$

where K_i is the number of differential time spikes with difference i as seen in Fig. 1. The resulting plot of $B_S(b)$ for different values of b can be seen in Fig. 2, which shows that the bit width for the differential time encoding leading to the least amount of bits required, is 2.

When analyzing the three discussed encodings: absolute, sampled or differential, we gave reasons in terms of efficiency advocating for differential time encoding. Considering implementation of neuron processing, one might have reservations for differential time encoded representations as one has to determine across different spike trains which spike to process next in chronological order. Although this is trivial for absolute time encoded and sampled sequences, it is not obvious for differential time encoded spike trains where ordering is given within a spike sequence, but is not guaranteed across different sequences. However, as we show in the next section, such order can be restored by a simple procedure without the need for conversion to other representations.

IV. Comparing spike trains in differential time

In the following, we show that multiple differential time encoded spike sequences can be merged without calculating the cumulative sums first and subsequently merging the sequences in absolute time. We describe the proof for two sequences, since it can trivially be extended to any number of sequences.

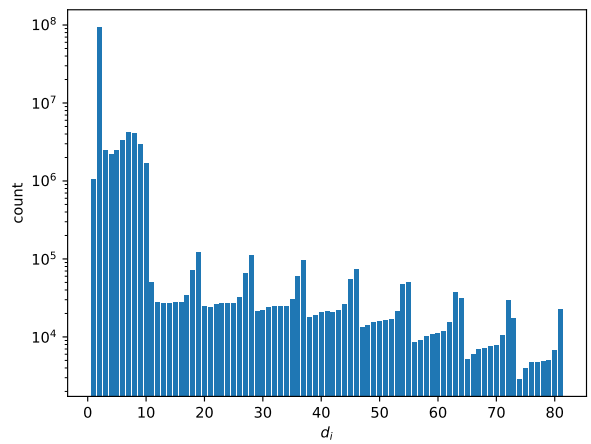

Fig. 1. Histogram for the difference times when using the test set of the MNIST dataset with 9x9 learned encoding as shown in Section VII.

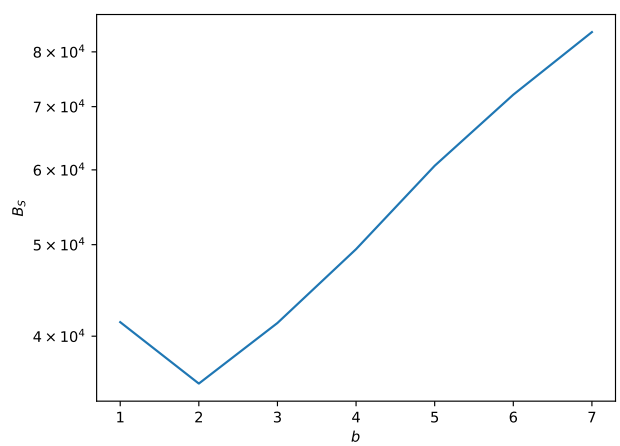

Fig. 2. Overall number of bits B_S required to encode the entire spike train based on chosen bit width b for the differential time.

Let $(A = \{a_i\}_{i=1}^n, \leq)$ be the ordered set of the absolute spike times of a spike train (the most commonly used ordering of ordered sets is the natural ordering of time values), and $(B = \{b_j\}_{j=1}^m, \leq)$ an ordered set of absolute spike times of a second spike train, defined in the same way. Note that for clarity all spikes and spike trains given in differential time in this section will be prefixed by Δ in order to avoid confusion. All other spikes are assumed to be given in absolute time unless stated otherwise.

The ordered sets of differential times are then defined such that $(\Delta A = \{\Delta a_i = a_i - a_{i-1}\}_{i=1}^n, a_{i-1} \leq a_i)$ using $a_0 = 0$.

The merged sequence $Y = A \cup B$ is realized by the order relation. Its ordered set of differential times ΔY is again defined in the same way as described for ΔA above. The cumulative sum of the elements of ΔY will again give Y.

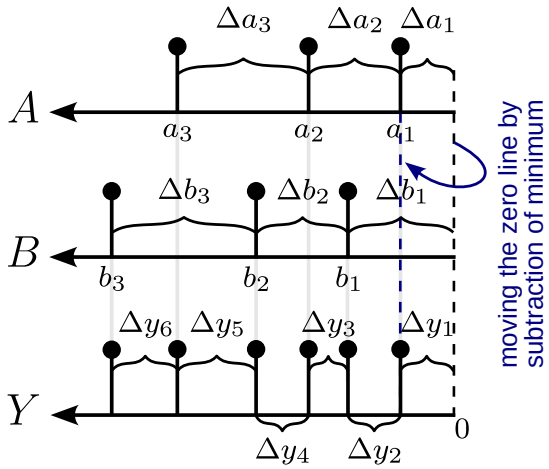

Fig. 3. Merging of spike sequences given in differential time.

Proposition 1. *The ordered set ΔY can be generated directly from ΔA and ΔB using the following procedure: Compare the first elements of the input sets ΔA and ΔB to each other. Append the minimum to the output set ΔY, remove the minimum from its respective set, and update the other first element (when using more than two sets: update all the other first elements) by subtracting the minimum from it. Repeat until all input sets are empty.*

Proof. Proofing the above proposition can be easily done based on the observation that the first elements of differential time encoded sets are in absolute relation to each other as they can be interpreted as absolute times to a set zero time. See Fig. 3 for depiction. An ordering with respect to their difference times is guaranteed only for the first elements of the differential time encoded sets. This means that the first delta time of the merged spike train ΔY must be the minimal element among the first elements of the input spike trains. Updating the other first elements (in the general case of more than two spike trains) by subtracting this minimum time can be interpreted as moving the set zero timeline (i.e. resetting the timeline to a new shifted zero). After the subtractions, all first elements of the differential time-encoded input spike trains are in absolute relation again, although now with the shifted set time. Outputting the minimum elements gives the sequence ΔY. □

V. Hardware architecture

Having established that the differential time representation has benefits compared to other representations, the next step is to explore how this can be used in implementations for SNN inference. This work is an extension of the design in [5], which introduced a hardware architecture capable of accelerating feedforward SNNs consisting of any number of layers of arbitrary size using the standard LIF neuron, while also using differential time spikes as inputs and outputs. The standard version of the LIF neuron is given as

$$P_k = P_{k-1}\beta^{\Delta t} + \sum_i w_i s_i - s_{out}$$
$$s_{out} = \begin{cases} \theta, & \text{if } P \geq \theta \\ 0, & \text{if } P < \theta, \end{cases} \tag{6}$$

where $P \in \mathbb{R}$ is the neuron potential, $\beta \in [0, 1]$ is the decay rate of the potential, $\Delta t \in \mathbb{N}_0$ is the time that passed since the last event, $k \in \mathbb{N}_0$ is the time where at least one input spike $s_i \in \{0, 1\}$ occurred, $\sum_i w_i s_i$ is the weighted sum of the input spikes (at the current event) and their corresponding weights, $s_{out} \in \mathbb{R}$ is responsible for resetting the neuron potential after a spike is triggered and $\theta \in \mathbb{R}$ is the threshold. The authors assume here that $\beta = 0.5$, as it was shown by the same authors in [4] that this does not diminish the capability of the neuron, as well as $\theta = 1$. Therefore, the hardware only needs to be able to store the continuously changing values of the neuron potential P_k for each neuron, as well as the weights w_i, learned during the training stage of the network. As such, the hardware architecture needs a way to correctly find the earliest spike among all spike trains entering the network, as established in Section IV, in order to properly define Δt needed for decaying the neuron potential in (6).

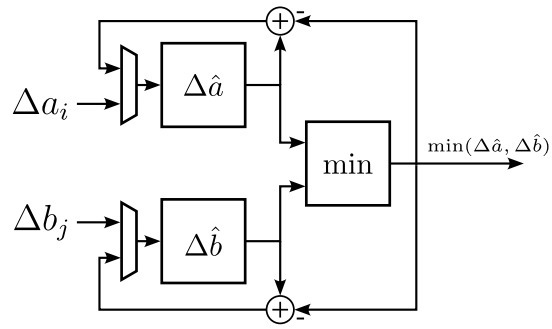

Fig. 4. Spike merger element capable of merging two separate spike trains given in differential time.

A. Merging the spikes in hardware

This merging of the spikes can be accomplished by directly implementing Proposition 1, leading to the spike merger element shown in Fig. 4, with the variables $\Delta\hat{a}$ and $\Delta\hat{b}$ representing the continuously updated Δa_i and Δb_j respectively. This update is either by subtraction or by replacement with the next difference time of the spike train.

The hardware block in Fig. 4 merges two separate spike trains given in differential time, producing a new spike train given in differential time, containing all spikes from both input spike trains. By cascading the spike merger elements, any number of spike trains can be efficiently combined into a single spike train, using a tree structure of depth $\lceil \log_2(M) \rceil$ with $M - 1$ spike merger elements, where M is the number of separate spike trains entering the network.

While this merger element allows finding the spike that occurs next, it obfuscates the information of which spike train produced that spike. This information is necessary for

selecting the weights that will later be added to the respective neuron potentials, since each spike train is assigned a separate set of weights during the training stage. Fortunately, finding the producing spike train can be solved relatively easily by introducing a separate vector which is extended by one bit during each stage of the $\log_2(M)$ tree. Depending if the upper or lower spike train produced the minimum for each spike merger element, either a 1 or a 0 is appended to the vector, thus producing an index identifying the originating spike train.

B. Processing the neuron layer

The spike merger tree is only needed once for the entire network, and receives all of the input spike trains. The produced differential time to the next spike, as well as the index of the producing spike train, i.e. the synapse index, are then sent into the first layer of the network. The synapse index can be used to directly address the weights in memory, providing the weights of all the synapses in the next layer which are connected to the synapse that produced the input spike. All retrieved weights are then handed in parallel to the respective neuron cores, which hold the neuron potential for every neuron in the layer. These weights are added directly to the neuron potential registers after which the thresholding operation and spike generation is handled by the neuron cores.
The layer controller in turn is responsible for processing the differential time produced by either the previous layer or the spike merger tree, in order to generate the control signals necessary for decaying the neuron potential in each core. Furthermore, it is also responsible for ensuring that the neuron cores generate spikes at the correct clock cycle, guaranteeing proper timing between layers, which also includes delaying the forwarding of the differential time until all spikes of the current layer have been processed (for LIF neurons, output spikes can only be triggered at times of input spikes). As each of the neuron cores produces only a single bit of information ($0 \rightarrow$ no spike, $1 \rightarrow$ spike), these bits are then fed into a Leading-One Position Detector (LOPD) [34]–[37], to once again arrive back at the index of a synapse that triggered a spike, which can be fed into the next layer. Therefore, each of the layers present in the network is directly instantiated in the hardware and can work in parallel to every other layer, as shown in Fig. 5.

VI. Synthesis Results

Complementary to the FPGA synthesis results that will be shown below, an ASIC synthesis run was also completed using the open-source OpenROAD software [38] and the accompanying OpenROAD-Flow-Scripts (ORFs). While there are quite a few open-source Process Design Kits (PDKs) available, such as the SKY130 and IHP 130nm PDK [39], there are now also predictive PDKs available for smaller technology nodes. One is the openly available ASAP7 PDK [8], which was used to run the synthesis for the design shown in Fig. 5. While the ORFs already provide built-in support for the ASAP7 PDK, a lot of other tools are necessary to complete the flow, e.g. KLayout and Yosys among others, all of which are thankfully provided in many pre-built Docker containers. The one chosen here is the container hosted by the Institute for Integrated Circuits and Quantum Computing at the Johannes Kepler University, which can be found in [40].

Apart from initially setting up the flow, another big issue compared to the FPGA implementation is the use of blockrams for storing the weights of the network. While readily available in modern FPGAs, synthesizing them using regular registers would not only be wasteful in terms of area and power, but has also resulted in non-terminating runtimes of the OpenROAD software, potentially due to diverging optimization runs during floorplanning and place & route optimization steps. Therefore, it is necessary to replace the blockrams with dedicated SRAM blocks, which are publicly available for the ASAP7 technology node [41], although they have not been in use widely, according to discussions with the maintainers. While the FPGA implementation can easily access multiple blockrams in parallel to achieve very wide, i.e. high-bit-width, access patterns, for the ASIC this means instantiating multiple SRAMs in order to achieve the same bit width. Theoretically it is possible to build SRAM blocks with very wide access patterns, however none of the open-source software tools available at the time of writing were capable of generating such SRAM blocks for the ASAP7 PDK. While it is possible to add logic to simply collect the necessary data over several clock cycles from a smaller number of SRAM blocks, this would have lessened the comparability of the ASIC to the FPGA implementation since quite a few modifications to the RTL would have been required. Therefore, it was chosen to simply instantiate multiple SRAM blocks in parallel, in order to achieve the necessary bit widths, which obviously leads to less than ideal floorplanning and routing, thus negatively influencing the performance and power requirements of the chip. The final layout of the entire chip can be seen in Fig. 6, with the respective areas and color coding shown in Tab. I. Note that we consider the results for the ASIC synthesis in terms of clock speed and area, as informative bounds. With optimized SRAM blocks we expect that the clock speed can be significantly increased and the area further reduced. This also becomes evident when looking at the power consumption for the ASIC shown in Tab. II, which highlights the fact that the macros, i.e. the SRAM blocks, are responsible for more than 67% of the total power consumption of the chip, as well as $\approx 30\%$ of the total area. In contrast, the entirety of the combinational and sequential design uses up a mere $\approx 3.7\%$ of the entire area and $\approx 18.7\%$ of the power (disregarding the power used for distributing the clock). Note that the ASIC flow was only completed for the accelerator structure optimized for the MNIST dataset, since the Cifar-10 version would have required even more SRAM blocks, which the current verson of the flow scripts did not allow to be placed.

VII. Learning the Encoding

The hardware described in Section V processes spikes given in differential time, however, this representation does not match the data that is often given as equidistantly spaced vector data, such as pixel maps obtained from cameras. Although

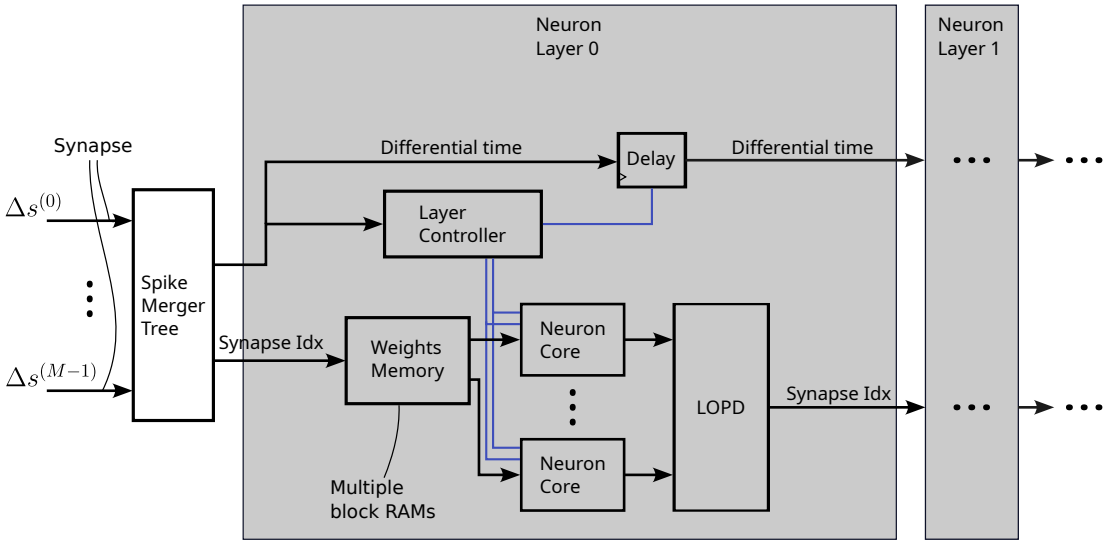

Fig. 5. Hardware architecture capable of accelerating arbitrarily deep and wide feedforward networks of LIF neurons [5].

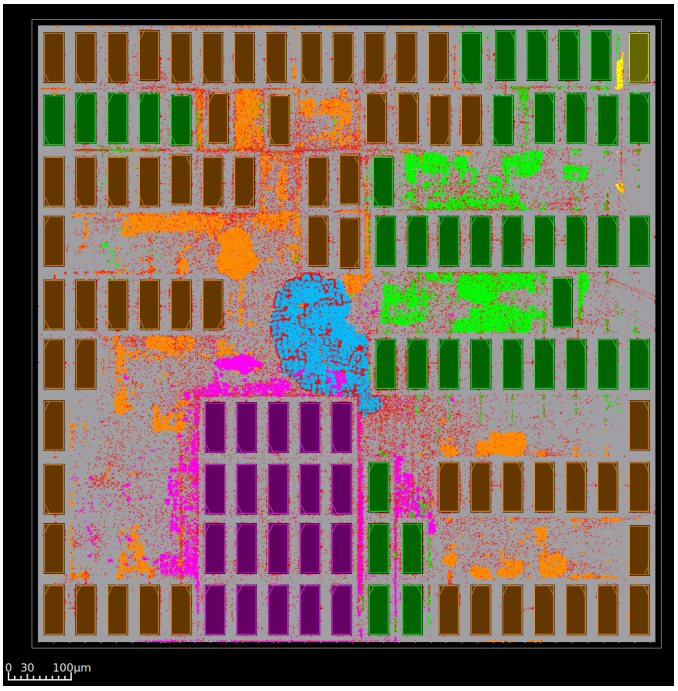

Fig. 6. ASIC layout using open-source ORFs and ASAP7 PDK with 124 SRAM blocks of size 64x1024 bits for a fully connected feedforward network of size 400-800-512-256-10. The color coding for the different blocks can be seen in Tab. I.

TABLE I
COLOR CODING AND RESPECTIVE AREA UTILIZATION FOR EACH COMPONENT OF FIG. 6.

Color	Component	Area	
	Top level	1.601e-03 mm^2	0.160%
	Spike Merger Tree	7.866e-03 mm^2	0.787%
	Layer 400-800	13.764e-03 mm^2	1.376%
	Layer 800-512	8.872e-03 mm^2	0.887%
	Layer 512-256	4.685e-03 mm^2	0.469%
	Layer 256-10	0.259e-03 mm^2	0.026%
	SRAM blocks	292.623e-03 mm^2	29.260%
	Total	328.069e-03 mm^2	32.807%

TABLE II
POWER REQUIREMENTS FOR THE ASAP7 CHIP RUNNING AT 538MHZ.

	Internal [W]	Switching [W]	Leakage [W]	Total [W]	
Sequential	2.53e-02	4.74e-04	6.97e-06	2.58e-02	9.8%
Combinational	8.93e-03	1.46e-02	5.36e-05	2.36e-02	8.9%
Clock	2.20e-02	1.39e-02	1.53e-06	3.59e-02	13.6%
Macro	1.79e-01	0.00e-00	0.00e-00	1.79e-01	67.7%
Total	2.35e-01	2.89e-02	6.21e-05	2.64e-01	100.0%

there are approaches for sensors that directly produce spikes, such as event-based cameras or level-crossing ADCs [46]–[48], usually the equidistantly sampled data needs to be converted into spike trains, a process that is referred to as encoding the data. While many different encoding methods have been proposed, with some of them having even been integrated into learning frameworks like SNNTorch [49], it is the responsibility of the user to choose the best encoding method for the given dataset and problem. The authors of this work propose to learn this encoding in conjunction with the network weights during the training process of the network. For image based datasets such as MNIST [6] or Cifar-10 [7] this is accomplished by selecting square patches from the pixels, which are then serialized. The serialized pixel values are then immediately fed into a LIF neuron that is responsible for the encoding, as can be seen in Fig. 7. Inside the network, typically the inputs to the LIF neuron are in the set $\{0, 1\}$, thus making multiplication with the weights unnecessary. However, when the pixel values are directly used as inputs, learning the weights would require multiplications, which is undesirable from an area and power perspective if the encoding is to be included in the accelerator. Therefore, the weights to be learned by the network have to be restricted to the set $\{-1, 0, 1\}$, thus only requiring addition and subtraction.

TABLE III
COMPARISON TO OTHER HARDWARE ACCELERATOR ARCHITECTURES.

Work	Process	Dataset	Accuracy [%]	Inferences/sec	Clock freq. [MHz]	Area [mm²]	#Multipliers	Power [W]
This work	ASAP7	MNIST	**99.03**	≈ 6000	**538**	**1**	**0**	0.26
[42]	10nm FinFET CMOS	MNIST	97.9	**6250**	509	1.99	N/R†	0.006*
[43]	130nm L130E	MNIST	95.01	≈ 50	150	102	N/R†	≈ 0.5
[44]	65nm LP CMOS	MNIST	97.6	2	0.07	1.72	N/R†	**0.3e-6**

Work	FPGA	Dataset	Accuracy [%]	Inferences/sec	Clock freq. [MHz]	#LUTs	#DSP blocks	Power [W]
This work [5]	ZCU102	MNIST	99.03	≈ **3400**	**300**	**56520**	**0**	**2.44**
[26]	ZCU102	MNIST	**99.60**	1631	200	224690	555	N/R†
[45]	XCZU9EG	MNIST	99.20	2124	125	155952	1795	4.5
This work	ZCU102	Cifar-10	55.15	≈ 2500	252	149445	**0**	6.63
[26]	ZCU102	Cifar-10	90.8	62	200	N/R†	N/R†	N/R†

† Not reported
* Uses separate power domain with different voltage and clock gating of unused SRAM cells to reduce power

While this restriction does negatively influence the accuracy achieved with the encoding, the difference is almost negligible according to our results (see [5]). The results when using the learned encoding on the MNIST and Cifar-10 test datasets respectively, can be seen in Tab. III.
As one can see from the ASIC synthesis results, the proposed design is superior in terms of accuracy for the MNIST data set, while maintaining low area / resource requirements. Although the energy requirements are higher than the comparison works, we also incorporate the power of the SRAM blocks into our calculations (one could further use methods from [42] to reduce the power consumption of the memory blocks as well). For the compared FPGA implementations, the proposed work is the fastest, both achieving the highest clock frequency and also the largest number of inferences/second while requiring no DSP blocks and using the least power. Meanwhile, the accuracy results for the proposed implementation is close to the top results of the compared works. Although the results for the Cifar-10 dataset are well below the maximum reported accuracies, they coincide with typical accuracy values for feedforward ANNs [50], [51]. As a future task, it remains to be investigated how to incorporate convolutional-like layers in SNNs with low complexity while maintaining high accuracy.

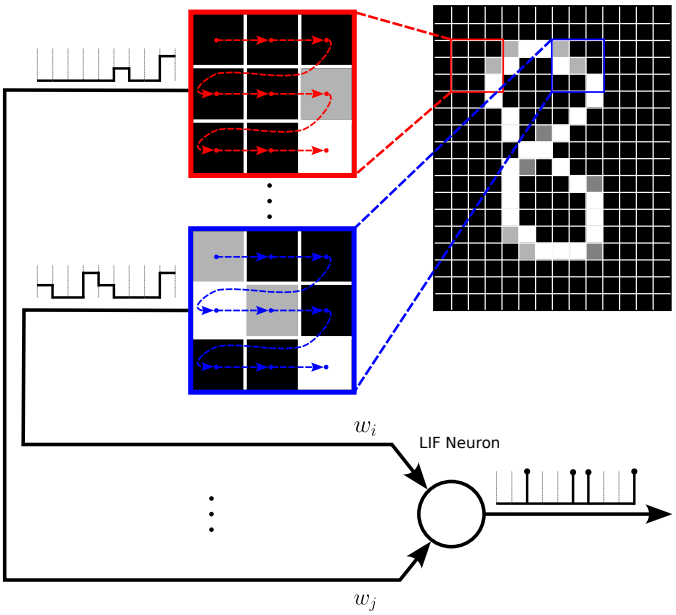

Fig. 7. 3x3 learned encoding by using patch-wise selection of the pixels with subsequent neuron activation [5].

VIII. CONCLUSION

This work discusses different ways for representing spike trains and their respective advantages and disadvantages. It establishes that the previously presented differential time encoding used to encode spike trains has many advantages compared to the absolute time and sampled representation. The spike merger is introduced as a way to join disparate spike trains, with an accompanying efficient hardware design, which serves as the entrypoint to the presented SNN accelerator architecture. Synthesis results for a Xilinx Ultrascale+ FPGA are shown, as well as ASIC design results using the open-source 7nm ASAP7 PDK alongside a fully open-source software stack and flow. These results clearly show that the design achieves superior accuracy on the MNIST dataset compared to other works, while maintaining low resource requirements.

ACKNOWLEDGMENTS

This research received funding from the Austrian Research Promotion Agency (FFG) and the Austrian ministry for Climate Action, Environment, Energy, Mobility, Innovation and Technology (BMK) under project no. FO999899263 and funding from the Chips Joint Undertaking under project no. 101112274 (ISOLDE) and its members Austria, Czechia, France, Germany, Italy, Romania, Spain, Sweden, Switzerland.

This work is furthermore supported by: the COMET-K2 “Center for Symbiotic Mechatronics” of the Linz Center of Mechatronics (LCM), funded by the Austrian federal government and the federal state of Upper Austria.

REFERENCES

[1] OpenAI, J. Achiam, S. Adler, S. Agarwal *et al.*, "Gpt-4 technical report," 2024. [Online]. Available: https://arxiv.org/abs/2303.08774

[2] M. Dampfhoffer, T. Mesquida, A. Valentian, and L. Anghel, "Are snns really more energy-efficient than anns? an in-depth hardware-aware study," *IEEE Transactions on Emerging Topics in Computational Intelligence*, vol. 7, no. 3, pp. 731–741, 2023.

[3] B. A. Moser and M. Lunglmayr, "On the sampling sparsity of analog-to-spike conversion based on leaky integrate-and-fire," *Neuromorphic Computing and Engineering*, vol. 5, no. 1, p. 014011, mar 2025. [Online]. Available: https://dx.doi.org/10.1088/2634-4386/adb884

[4] D. Windhager, B. A. Moser, and M. Lunglmayr, "Snn architecture for differential time encoding using decoupled processing time," 2023. [Online]. Available: https://arxiv.org/abs/2311.14447

[5] D. Windhager, L. Ratschbacher, B. A. Moser, and M. Lunglmayr, "Spiking neural network accelerator architecture for differential-time representation using learned encoding," accepted for publication in Proc. of ISCAS2025. [Online]. Available: https://arxiv.org/abs/2501.07952

[6] Y. LeCun, C. Cortes, and C. Burges, "MNIST Handwritten Digit Database," 2010. [Online]. Available: http://yann.lecun.com/exdb/mnist

[7] A. Krizhevsky, "Learning multiple layers of features from tiny images," 2009. [Online]. Available: https://api.semanticscholar.org/CorpusID:18268744

[8] L. T. Clark, V. Vashishtha, L. Shifren, A. Gujja, S. Sinha, B. Cline, C. Ramamurthy, and G. Yeric, "Asap7: A 7-nm finfet predictive process design kit," *Microelectronics Journal*, vol. 53, pp. 105–115, 2016. [Online]. Available: https://www.sciencedirect.com/science/article/pii/S002626921630026X

[9] Z. Hao, Y. Huang, Z. Xu, Z. Yu, and T. Huang, "Comprehensive online training and deployment for spiking neural networks," 2024. [Online]. Available: https://arxiv.org/abs/2410.07547

[10] P. Qu, H. Lin, M. Pang, X. Liu, W. Zheng, and Y. Zhang, "Enlarge: An efficient snn simulation framework on gpu clusters," *IEEE Transactions on Parallel and Distributed Systems*, vol. 34, no. 9, pp. 2529–2540, 2023.

[11] A. Ahmadi and H. Soleimani, "A gpu based simulation of multilayer spiking neural networks," in *2011 19th Iranian Conference on Electrical Engineering*, 2011, pp. 1–1.

[12] Y. Li, J. Li, K. Sun, L. Leng, and R. Cheng, "Towards scalable gpu-accelerated snn training via temporal fusion," 2024. [Online]. Available: https://arxiv.org/abs/2408.00280

[13] S. Hassan, M. Inouye, M. C. Gonzalez, I. Aliyev, J. Mack, M. Hafiz, and A. Akoglu, "Gpu-ranc: A cuda accelerated simulation framework for neuromorphic architectures," 2024. [Online]. Available: https://arxiv.org/abs/2404.16208

[14] M. Davies, N. Srinivasa, T.-H. Lin, G. Chinya, Y. Cao, S. H. Choday, G. Dimou, P. Joshi, N. Imam, S. Jain, Y. Liao, C.-K. Lin, A. Lines, R. Liu, D. Mathaikutty, S. McCoy, A. Paul, J. Tse, G. Venkataramanan, Y.-H. Weng, A. Wild, Y. Yang, and H. Wang, "Loihi: A neuromorphic manycore processor with on-chip learning," *IEEE Micro*, vol. 38, no. 1, pp. 82–99, 2018.

[15] S. B. Furber, F. Galluppi, S. Temple, and L. A. Plana, "The spinnaker project," *Proceedings of the IEEE*, vol. 102, no. 5, pp. 652–665, 2014.

[16] C. Mayr, S. Hoeppner, and S. Furber, "Spinnaker 2: A 10 million core processor system for brain simulation and machine learning," 2019. [Online]. Available: https://arxiv.org/abs/1911.02385

[17] Z. Yan, Z. Bai, T. Mitra, and W.-F. Wong, "Sparrowsnn: A hardware/software co-design for energy efficient ecg classification," 2024. [Online]. Available: https://arxiv.org/abs/2406.06543

[18] G. Moody and R. Mark, "The impact of the mit-bih arrhythmia database," *IEEE Engineering in Medicine and Biology Magazine*, vol. 20, no. 3, pp. 45–50, 2001.

[19] J. Song, J. Shin, H. Kim, and W.-S. Choi, "Energy-efficient high-accuracy spiking neural network inference using time-domain neurons," 2022. [Online]. Available: https://arxiv.org/abs/2202.02015

[20] A. Aydin, M. Gehrig, D. Gehrig, and D. Scaramuzza, "A hybrid ann-snn architecture for low-power and low-latency visual perception," 2024. [Online]. Available: https://arxiv.org/abs/2303.14176

[21] S. Haghighatshoar and D. R. Muir, "Low-power spiking neural network audio source localisation using a hilbert transform audio event encoding scheme," *Communications Engineering*, vol. 4, no. 1, Feb. 2025. [Online]. Available: http://dx.doi.org/10.1038/s44172-025-00359-9

[22] A. H. Ali, M. Navardi, and T. Mohsenin, "Energy-aware fpga implementation of spiking neural network with lif neurons," 2024. [Online]. Available: https://arxiv.org/abs/2411.01628

[23] M. T. L. Aung, D. Gerlinghoff, C. Qu, L. Yang, T. Huang, R. S. M. Goh, T. Luo, and W.-F. Wong, "Deepfire2: A convolutional spiking neural network accelerator on fpgas," *IEEE Transactions on Computers*, vol. 72, no. 10, p. 2847–2857, Oct. 2023. [Online]. Available: http://dx.doi.org/10.1109/TC.2023.3272284

[24] H. Liu, Y. Chen, Z. Zeng, M. Zhang, and H. Qu, "A low power and low latency fpga-based spiking neural network accelerator," in *2023 International Joint Conference on Neural Networks (IJCNN)*, 2023, pp. 1–8.

[25] J. Li, G. Shen, D. Zhao, Q. Zhang, and Y. Zeng, "Firefly: A high-throughput hardware accelerator for spiking neural networks with efficient dsp and memory optimization," *IEEE Transactions on Very Large Scale Integration (VLSI) Systems*, vol. 31, no. 8, pp. 1178–1191, 2023.

[26] S. Panchapakesan, Z. Fang, and J. Li, "Syncnn: Evaluating and accelerating spiking neural networks on fpgas," in *2021 31st International Conference on Field-Programmable Logic and Applications (FPL)*, 2021, pp. 286–293.

[27] A. Khodamoradi, K. Denolf, and R. Kastner, "S2n2: A fpga accelerator for streaming spiking neural networks," in *The 2021 ACM/SIGDA International Symposium on Field-Programmable Gate Arrays*, ser. FPGA '21. New York, NY, USA: Association for Computing Machinery, 2021, p. 194–205. [Online]. Available: https://doi.org/10.1145/3431920.3439283

[28] Y. Nevarez, D. Rotermund, K. R. Pawelzik, and A. Garcia-Ortiz, "Accelerating spike-by-spike neural networks on fpga with hybrid custom floating-point and logarithmic dot-product approximation," *IEEE Access*, vol. 9, pp. 80 603–80 620, 2021.

[29] Q. Liu, G. Pan, H. Ruan, D. Xing, Q. Xu, and H. Tang, "Unsupervised aer object recognition based on multiscale spatio-temporal features and spiking neurons," *IEEE Transactions on Neural Networks and Learning Systems*, vol. 31, no. 12, pp. 5300–5311, 2020.

[30] T. Mesquida, A. Valentian, D. Bol, and E. Beigne, "Impact of the aer-induced timing distortion on spiking neural networks implementing dsp," in *2016 12th Conference on Ph.D. Research in Microelectronics and Electronics (PRIME)*, 2016, pp. 1–4.

[31] J. Kim, J. Park, S. Joo, and S.-O. Jung, "Efficient hardware implementation of stdp for aer based large-scale snn neuromorphic system," in *2020 35th International Technical Conference on Circuits/Systems, Computers and Communications (ITC-CSCC)*, 2020, pp. 1–4.

[32] M. S. R, S. Chakrabartty, and C. S. Thakur, "Neuromorphic computing with aer using time-to-event-margin propagation," 2023. [Online]. Available: https://arxiv.org/abs/2304.13918

[33] M. Lunglmayr, G. Lindorfer, and B. Moser, "Robust and efficient bio-inspired data-sampling prototype for time-series analysis," in *DEXA 2021*. Springer International Publishing, 2021, pp. 119–126.

[34] M. S. Ansari, S. Gandhi, B. F. Cockburn, and J. Han, "Fast and low-power leading-one detectors for energy-efficient logarithmic computing," *IET Computers & Digital Techniques*, vol. 15, no. 4, pp. 241–250, 2021. [Online]. Available: https://ietresearch.onlinelibrary.wiley.com/doi/abs/10.1049/cdt2.12019

[35] K. Kunaraj and R. Seshasayanan, "Leading one detectors and leading one position detectors - an evolutionary design methodology," *Canadian Journal of Electrical and Computer Engineering*, vol. 36, no. 3, pp. 103–110, 2013.

[36] K. Abed and R. Siferd, "Vlsi implementations of low-power leading-one detector circuits," in *Proceedings of the IEEE SoutheastCon 2006*, 2006, pp. 279–284.

[37] S. Gandhi, M. S. Ansari, B. F. Cockburn, and J. Han, "Approximate leading one detector design for a hardware-efficient mitchell multiplier," in *2019 IEEE Canadian Conference of Electrical and Computer Engineering (CCECE)*, 2019, pp. 1–4.

[38] T. Ajayi, V. A. Chhabria, M. Fogaça, S. Hashemi, A. Hosny, A. B. Kahng, M. Kim, J. Lee, U. Mallappa, M. Neseem *et al.*, "Toward an open-source digital flow: First learnings from the openroad project," in *Proceedings of the 56th Annual Design Automation Conference 2019*, 2019, pp. 1–4.

[39] K. Herman, N. Herfurth, T. Henkes, S. Andreev, R. Scholz, M. Müller, M. Krattenmacher, H. Pretl, and W. Grabinski, "On the versatility of the ihp bicmos open source and manufacturable pdk: A step towards the future where anybody can design and build a chip," *IEEE Solid-State Circuits Magazine*, vol. 16, no. 2, pp. 30–38, 2024.

[40] H. Pretl and G. Zachl, "GitHub repository of the IIC-OSIC-TOOLS," Sep. 2023. [Online]. Available: https://github.com/iic-jku/IIC-OSIC-TOOLS

[41] V. Vashishtha, M. Vangala, P. Sharma, and L. T. Clark, "Robust 7-nm sram design on a predictive pdk," in *2017 IEEE International Symposium on Circuits and Systems (ISCAS)*, 2017, pp. 1–4.

[42] G. K. Chen, R. Kumar, H. E. Sumbul, P. C. Knag, and R. K. Krishnamurthy, "A 4096-neuron 1m-synapse 3.8-pj/sop spiking neural network with on-chip stdp learning and sparse weights in 10-nm finfet cmos," *IEEE Journal of Solid-State Circuits*, vol. 54, no. 4, pp. 992–1002, 2019.

[43] E. Stromatias, D. Neil, F. Galluppi, M. Pfeiffer, S.-C. Liu, and S. Furber, "Scalable energy-efficient, low-latency implementations of trained spiking deep belief networks on spinnaker," in *2015 International Joint Conference on Neural Networks (IJCNN)*, 2015, pp. 1–8.

[44] P. K. Chundi, D. Wang, S. J. Kim, M. Yang, J. P. Cerqueira, J. Kang, S. Jung, S. Kim, and M. Seok, "Always-on sub-microwatt spiking neural network based on spike-driven clock- and power-gating for an ultra-low-power intelligent device," *Frontiers in Neuroscience*, vol. Volume 15 - 2021, 2021. [Online]. Available: https://www.frontiersin.org/journals/neuroscience/articles/10.3389/fnins.2021.684113

[45] H. Fang, Z. Mei, A. Shrestha, Z. Zhao, Y. Li, and Q. Qiu, "Encoding, model, and architecture: Systematic optimization for spiking neural network in fpgas," in *2020 IEEE/ACM International Conference On Computer Aided Design (ICCAD)*, 2020, pp. 1–9.

[46] M. Lunglmayr, G. Lindorfer, and B. Moser, "Robust and efficient bio-inspired data-sampling prototype for time-series analysis," in *Database and Expert Systems Applications - DEXA 2021 Workshops*. Cham: Springer International Publishing, 2021, pp. 119–126.

[47] Y. Hou, J. Qu, Z. Tian, M. Atef, K. Yousef, Y. Lian, and G. Wang, "A 61-nw level-crossing adc with adaptive sampling for biomedical applications," *IEEE Transactions on Circuits and Systems II: Express Briefs*, vol. 66, no. 1, pp. 56–60, 2019.

[48] A. Ogweno, P. Degenaar, V. Khomenko, and A. Yakovlev, "A fixed window level crossing adc with activity dependent power dissipation," in *2016 14th IEEE International New Circuits and Systems Conference (NEWCAS)*, 2016, pp. 1–4.

[49] J. K. Eshraghian, M. Ward, E. Neftci, X. Wang, G. Lenz, G. Dwivedi, M. Bennamoun, D. S. Jeong, and W. D. Lu, "Training spiking neural networks using lessons from deep learning," *Proceedings of the IEEE*, vol. 111, no. 9, pp. 1016–1054, 2023.

[50] V. Krikonis, "Cifar-10 analysis with a neural network," https://www.kaggle.com/code/vassiliskrikonis/cifar-10-analysis-with-a-neural-network, 2021, accessed: 2025-04-28.

[51] A. Jahantab, "Cifar-10 classification using linear models, ann, and cnn," https://github.com/amirjahantab/CIFAR-10, 2023, accessed: 2025-04-28.